408

ON THE VALIDITY OF THE BOUSSINESQ APPROXIMATION IN A TALL DIFFERENTIALLY HEATED CAVITY WITH WATER

D. Kizildag, I. Rodríguez, A. Oliva
Centre Tecnològic de Transferència de Calor (CTTC)
Universitat Politècnica de Catalunya (UPC)
ETSEIAT, Colom 11, 08222, Terrassa, Barcelona, Spain
Fax: +34 93 739 89 20 E-mail: cttc@cttc.upc.edu

ABSTRACT

In the present work, the fluid flow and heat transfer inside an integrated solar collector installed on an advanced façade are investigated. According to Gray and Giorgini [1], the use of the Boussinesq approximation can be considered valid for variations of thermosphysical properties up to 10 % with respect to the mean value. In the configuration under study, there is a variation of about 20 % in the dynamic viscosity and 15 % in the thermal expansion coefficient. Thus, the main objective of this work is to analyse the validity of the Boussinesq approximation for the turbulent natural convection flow of water in a rectangular parallelepiped tank. The significance of the Boussinesq effects is studied comparatively by means of detailed DNS simulations.

INTRODUCTION

The natural convection flow within enclosures has attracted the attention of many researchers due to its potential to model numerous applications of engineering interest, such as cooling of electronic devices, air flow in buildings, heat transfer in solar collectors, among others. The natural convection studies corresponding to the parallelepipedic enclosures can be classified into two elementary classes: i) heating from a horizontal wall (heating from below); ii) heating from a vertical wall. The characteristic example of the former case is the Rayleigh-Bénard flow, however this work will only focus on the cavities heated from the side. This configuration is referred commonly as the differentially heated cavity.

Although the differentially heated cavity configuration represents a simple geometry, the flow gets complex for sufficiently large Rayleigh numbers [2]. The flow undergoes a gradual transition to a chaotic state as the Rayleigh number reaches a critical value. For the situation studied in this work, both laminar, transitional, and turbulent zones are expected to coexist within the domain. Generally the core of the cavity together with the upstream part of the vertical boundary layers remain laminar while at some point in the downstream part of the vertical boundary layers, turbulent fluctuations become significant. It is a challenging task to detect this phenomenon [3]. Another important issue is the stratification phenomenon taking place in the core of the cavity. It is one of the basic open problems of this configuration. Comparisons between numerical and experimental studies give quite different results, which may be justified by the thermal radiation effects [4].

The vast majority of the performed work in this field corresponds to air-filled cavities (see [3] for a detailed preview). If the working fluid is water, obtaining solutions for the governing equations gets even more complicated, as the boundary layer becomes thinner than for air at the same conditions. As a consequence, there is an increasing demand for excessively fine grids in space and time for solving the three-dimensional and time dependent flow, in order to capture the smallest scales of the turbulent flow.

Additional to the issues explained above, when investigating the fluid behaviour in real working conditions,

the validity of the Boussinesq approximation has to be questioned. According to Gray and Giorgini [1], the use of the Boussinesq approximation can be considered valid for variations of thermosphysical properties up to 10% with respect to the mean value.

The main objective of this work is to analyze the turbulent natural convection flow of water in a rectangular parallelepiped tank. This configuration corresponds to an integrated solar collector installed on an advanced façade. The aspect ratio is $\Gamma = 6.68$. The working conditions of the particular design yield a Rayleigh number of $Ra = 2.2 \times 10^{11}$ and a Prandtl number of $Pr = 3.44$. Long-term accurate statistical data by means of a DNS simulation is presented, investigating the characteristics of the turbulent flow within the differentially heated cavity. Some results of first and second order turbulent statistics are also presented. Based on a previous work [5] this works aims at obtaining more details about the Boussinesq effects in turbulent natural convection flow. The actual working conditions of the prototype point out a variation of about 20 % in the dynamic viscosity and 15 % in the thermal expansion coefficient. Thus, it is of interest to analyze some features of turbulent natural convection flow including Boussinesq effects.

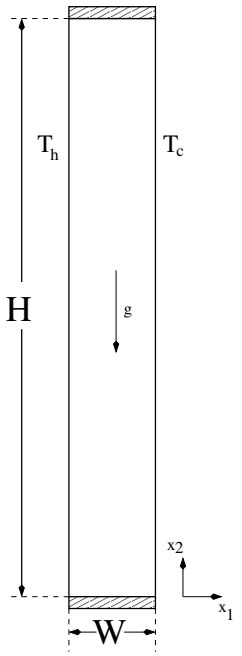

Figure 1: Geometry of the differentially heated cavity

CASE UNDER STUDY

The adopted geometry considered in this work is shown in Figure 1. This geometry models the parallelepiped tank of an integrated solar collector. The height of the tank (H), and the width (W) are 0.735m and 0.11m respectively, resulting in an aspect ratio of $\Gamma = 6.68$.

Taking into consideration the real working conditions of the studied prototype, the temperatures at the hot and cold vertical isothermal walls are set to 57 $^{\circ}C$ and 47 $^{\circ}C$ respectively.

DESCRIPTION OF THE MATHEMATICAL AND NUMERICAL METHOD

The Navier-Stokes and continuity equations can be written as

$$\mathsf{M}u = 0 \quad (1)$$

$$\frac{\partial u}{\partial t} + \mathsf{C}(u)\,u + \nu \mathsf{D}u + \rho^{-1}\mathsf{G}p + f = 0 \quad (2)$$

$$\frac{\partial \mathbf{T}}{\partial t} + \mathsf{C}(u)\,\mathbf{T} + \rho^{-1}Cp^{-1}k\mathsf{D}(\mathbf{T}) = 0 \quad (3)$$

where $u \in \mathbb{R}^{3m}$ and $p \in \mathbb{R}^{m}$ are the velocity vector and pressure, respectively (here m applies for the total number of control volumes (CV) of the discretised domain), ν is the kinematic viscosity and ρ the density. f is the body force $f = \beta(T_0 - T_m)g$. Convective and diffusive operators in the momentum equation for the velocity field are given by $\mathsf{C}(u) = (u \cdot \nabla) \in \mathbb{R}^{3m\times 3m}$, $\mathsf{D} = \nabla^2 \in \mathbb{R}^{3m\times 3m}$ respectively. Gradient and divergence (of a vector) operators are given by $\mathsf{G} = \nabla \in \mathbb{R}^{3m\times 3m}$ and $\mathsf{M} = \nabla\cdot \in \mathbb{R}^{m\times 3m}$ respectively.

In bouyancy driven flows a common approach is to consider constant thermophysical properties of the fluid, with the exception of the density variations that are only taken into account in the bouyancy forces, i.e., the so-called Oberbeck-Boussinesq approximation. Thus, the temperature dependency of density is linearized in the bouyancy force as:

$$\rho(T) = \rho_m - \rho_m \beta_m (\mathbf{T} - T_m) \quad (4)$$

Here $T_m = (T_h + T_c)/2$ is the mean value of the temperatures of the cold and hot walls. Those assumptions

have its own implications. First, continuity equation is treated in its incompressible form, neglecting acoustic phenomena, which in the case of liquids has no major implications. However, for liquids, deviations from the aforementioned hypothesis are mainly due to viscosity variations, as the viscosity strongly decreases with the temperature increase.

When considering the Boussinesq effects in our work, the following are assumed:

- temperature dependent thermophysical properties
- density variations are only taken into account in the bouyancy term
- the temperature dependence of the density is linearized as:

$$\rho(T) = \rho_m - \rho'(T) \tag{5}$$

Under the above assumptions, equations 1-3 read:

$$\mathsf{M}u = 0 \tag{6}$$

$$\frac{\partial u}{\partial t} + \mathsf{C}(u)\,u + \mathsf{D}(\nu(T)u) + \rho_m^{-1}\widehat{\mathsf{G}}p - \rho_m^{-1}\rho'(T)\mathbf{g} = 0 \tag{7}$$

$$\frac{\partial \mathbf{T}}{\partial t} + \mathsf{C}(u)\,\mathbf{T} + \rho_m^{-1}Cp_m^{-1}\mathsf{D}(k(T)\mathbf{T}) = 0 \tag{8}$$

The temperature dependencies for $\nu(T)$, $k(T)$ and $\rho(T)$ are taken from Furukawa.[6]

Considering the reference scales for length, time, velocity, temperature and dynamic pressure as H, $(H^2/\alpha)Ra^{-0.5}$, $(\alpha/H)Ra^{0.5}$, $T_h - T_c$, $\rho(\alpha/H^2)Ra$, respectively, Non-Oberbeck-Boussinesq thermal convection in the cavity is governed by the non-dimensional quantities: $Ra = (g\beta_m \Delta T_{ref} H^3 Pr_m)/\nu_m^2$, $Pr_m = \nu_m/\alpha_m$, Γ and the non-dimensional thermophysical properties: $\nu* = \nu(T)/\nu_m$; $k^* = k(T)/k_m$; $\rho^* = \frac{\rho_m - \rho(T)}{\rho_m \beta_m \Delta T_{ref}} = \frac{\rho'(T)}{\rho_m \beta_m \Delta T_{ref}}$.

The governing equations are discretized on a collocated unstructured grid arrangement, by means of second-order spectro-consistent schemes [7]. Such discretization preserves the symmetry properties of the continuous differential operators, i.e., the conservation properties are held if, the convective term is discretized by a skew-symmetric operator and the diffusive term is approximated by a symmetric, positive-definite coefficient matrix. These properties ensure both, stability and conservation of the global kinetic-energy balance on any grid. Energy transport is also discretized by means of a spectro-consistent scheme. An explicit third-order Gear-like scheme [8] based on a fractional step method is used for time-advancement algorithm, except for the pressure gradient where a first-order backward Euler scheme is used.

Collocated meshes do not conserve kinetic energy when fractional step method is used [9, 10]. The source of these errors are interpolation schemes and inconsistency in the pressure field, in order to ensure mass conservation. While the first is eliminated through the use of consevative schemes, the latter equals to $\varepsilon_{ke} = (\tilde{p_c})^* \mathsf{M}_c(\mathsf{G}_c - \mathsf{G}_s)\tilde{p_c}$. Felten and Lund [10] showed that pressure errors are of the order of $\mathscr{O}(\triangle x^2\, \triangle t)$. However, these errors do not have significant impact on the grid resolutions and time-steps used in DNS.

Boundary conditions and fluid properties: For the velocities, no-slip condition is applied on all the walls. In the spanwise direction (when applicable) periodic boundary condition is used.

Isothermal vertical walls are assumed. Left vertical wall is at 57 $^\circ C$ and right vertical wall is at 47 $^\circ C$. In the top and bottom confining walls, Neumann boundary condition ($\partial T/\partial n = 0$) is applied.

Except for the Non-Boussinesq calculations, the fluid properties for water are calculated at the average temperature of $(T_h + T_c)/2 = 52^\circ C$. Rayleigh number based on the height of the cavity is $Ra = \rho\beta(T_h - T_c)H^3/\nu\alpha = 2.2 \times 10^{11}$ and the Prandtl number is $Pr = \nu/\alpha = 3.44$, being ν is the kinematic viscosity and α thermal diffusivity.

In Figure 2 the temperature dependencies of density and kinematic viscosity are shown for the working temperatures of the prototype.

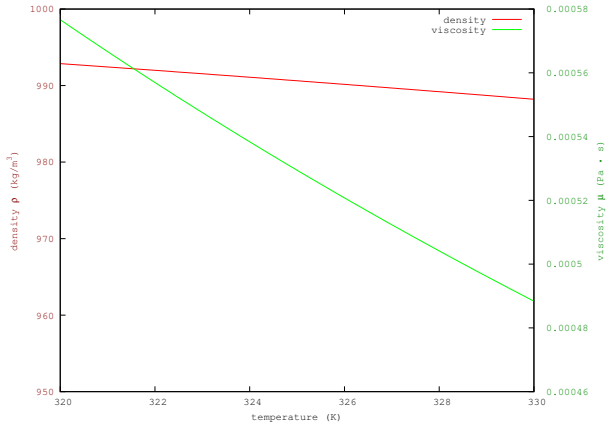

Figure 2: Variable thermophysical properties

Geometric discretization: The smallest scales at the hot and cold walls are imposed by viscous and thermal boundary layers, while grid size at the bulk must be lesser than Kolmogorov scale. For the Prandtl number in our case, the thermal boundary layer is thinner than the viscous boundary layer as $\delta_t \sim h/Ra^{0.25}$ and $\delta_v \sim Pr^{0.5}\delta_t$ [11]. The meshes shown in Table 1 are used for our preliminary studies.

Table 1: Space and time meshes used in the test cases.

mesh	m_2	m_3	m_4
N_x	258	314	535
N_y	770	940	1871
Δx_{min}	6.80×10^{-5}	6.80×10^{-5}	4.08×10^{-5}
Δy_{min}	1.30×10^{-3}	1.06×10^{-3}	5.34×10^{-4}
Δt	2.54×10^{-5}	2.54×10^{-5}	9.15×10^{-6}

PRELIMINARY RESULTS AND CONCLUSIONS

As the numerical effort to carry out the present simulations is too large, all the calculations here presented are restricted to two-dimensional (2D) simulations. Although 2D calculations might affect the fluid dynamics, some of the characteristics of the flow or the Boussinesq effects can still be captured under this assumption. It has been shown earlier by Trias et al. [3] for a differentially heated cavity for Rayleigh numbers up to 10^{10} and by Schalzl et al. [12] for Rayleigh-Benard convection, that in general as a rough approach to capture the general features of the flow and especially boundary layer profiles and Nusselt numbers, 2D simulations can be a good approximation.

In the present work, the results obtained for some of the mentioned meshes are presented, while results for other meshes are being calculated. In Table 2, a brief resume of the studied cases are shown.

Table 2: $\surd$ calculated cases; $\times$ pending cases.

mesh	Boussinesq (BSQ)	Non-Boussinesq (NBSQ)
m_2	$\surd$	$\surd$
m_3	$\surd$	$\times$
m_4	$\surd$	$\times$

In Figures 3 and 4 y-direction velocity profiles at mid height of the cavity are given. Boussinesq approximation solutions are symmetric in the vicinity of hot and cold walls, while the symmetry is broken in Non-Boussinesq solution. Even though the available Non-Boussinesq solution corresponds to the coarsest mesh level, the significant differences in y-direction velocities cannot be attributed to spatial discretization since the Boussinesq approximation solution for the same mesh gives acceptable results with respect to DNS solution.

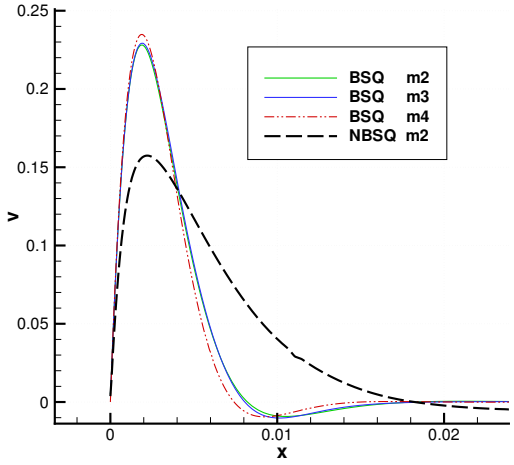

Figure 3: y-direction velocity profile at mid height of the cavity in the vicinity of hot wall

In the vicinity of the hot wall (see Figure 3), the Non-Boussinesq solution underestimates the peak value by approximately 35%. On the other hand, in the vicinity of the cold wall, Non-Boussinesq solution overestimates the absolute peak value by about 14 %. Morever, the peak values occur at different positions,

indicating differences in boundary layer thicknesses. For Non-Boussinesq solution, in hot wall the peak value corresponds to $x_{max} = 0.00217$ while for the finest mesh with Boussinesq approximation the peak occurs at$x_{max} = 0.0019$. In the cold wall, the values are 0.14768 and 0.147775 respectively.

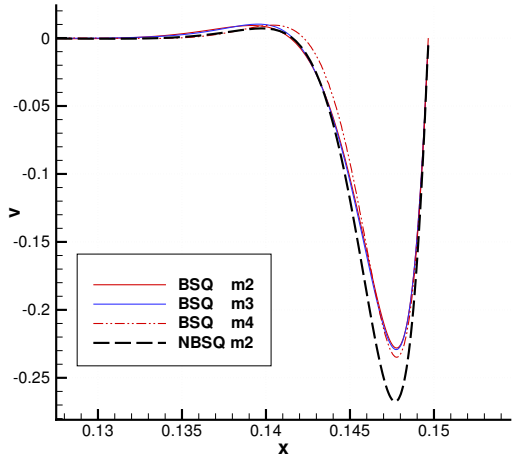

Figure 4: y-direction velocity profile at mid height of the cavity in the vicinity of cold wall

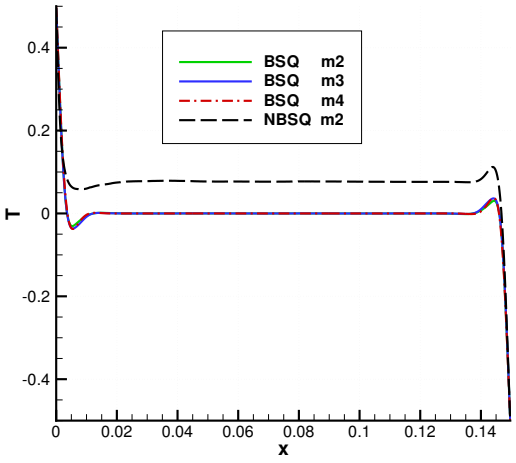

Figure 5: Temperature profiles at mid height of the cavity

As the core temperature is concerned, Non-Boussinesq solution predicts a significantly greater temperature ($T_c^{NBSQ} > T_c^{BSQ}$). This effect can be observed in Figure 5. In Boussinesq solution the temperature at the core of the cavity corresponds to the mean temperature of the case, however in Non-Boussinesq case this symmetry is broken.

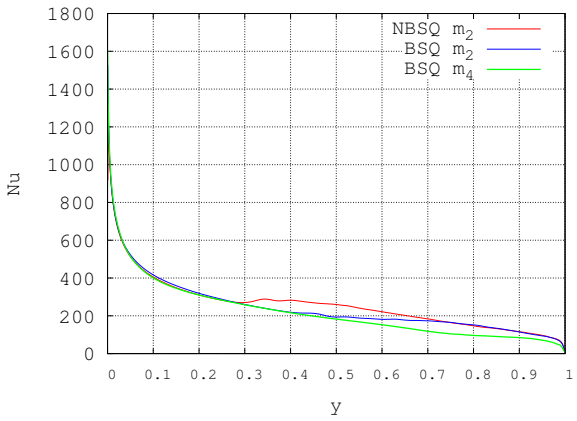

Figure 6: Local Nusselt number profile in hot wall

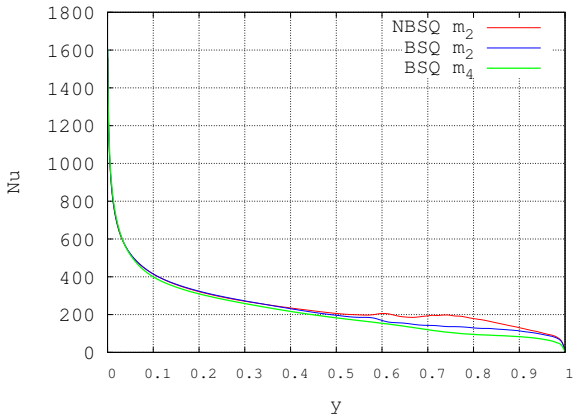

Figure 7: Local Nusselt number profile in cold wall

In Figure 6, the local Nusselt number distribution for both Boussinesq and Non-Boussinesq solutions are given for the coarsest mesh levels, and the reference DNS solution using Boussinesq approximation (BSQ m_4). This hot wall graph indicates different transition points. For Non-Boussinesq solution, the transition point is observed around $y = 0.35$ while as the Boussinesq approximation is adopted, the instabilities are not significant till approximately $y = 0.46$. These results show that the transition point estimation presents significant deviations, at least for the coarsest mesh. The average Nusselt numbers are shown in Table 3 with respect to the finest Boussinesq solution.

As we focus on the cold wall, the differences between Boussinesq and Non-Boussinesq solution in terms of transition point are less pronounced (see Figure 6). However, it is important to note that for the Non-Boussinesq solution the transition point corresponds

to $y = 0.60$, which clearly indicates the lack of symmetry in this case.

In Figures 8 and 9 the representative instantaneous isotherms corresponding to $t = 450$ and $t = 500$ are shown. Note that for the Non-Boussinesq solution, the core of the cavity is warmer than the Boussinesq solutions. Additionally, for this case the instabilities are visible in the vicinity of the hot wall by $1/3$ of the cavity, while in the case of the cold wall, we can roughly say that the instabilities are ejected to the core after 2/3 of the cavity length from the leading edge. However, both Boussinesq approximation solutions present symmetric behaviour as the instabilities are concerned. In the BSQ m_4 solution, the temperature drop in the top and bottom region occurs in a smaller region, which in turn makes relatively larger the mixing region in the core.

Table 3: Average Nusselt numbers

case	Average Nusselt	Error
NBSQ m_2	259.47	16.7 %
BSQ m_2	244.24	9.8 %
BSQ m_4	222.27	-

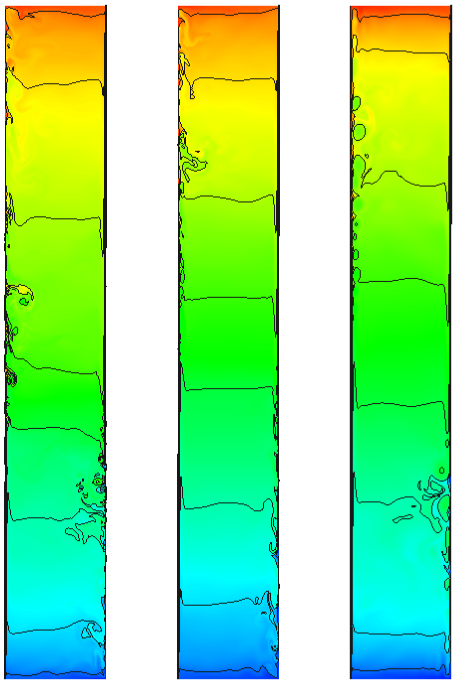

Figure 8: Representative instantaneous isotherms for t=450; (left) NBSQ m_2 , (middle) BSQ m_2, (right) BSQ m_4.

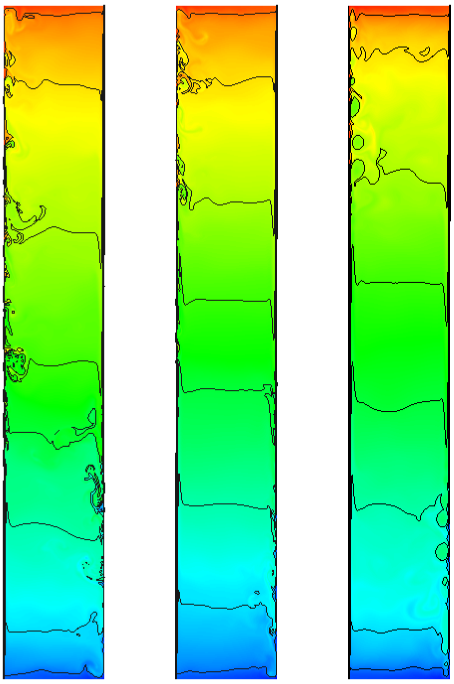

Figure 9: Representative instantaneous isotherms for t=500; (left) NBSQ m_2 , (middle) BSQ m_2, (right) BSQ m_4.

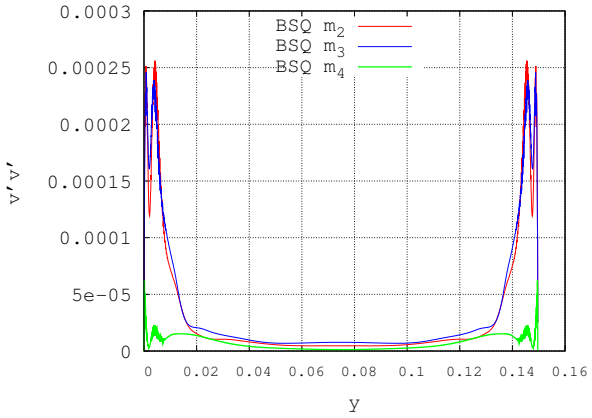

Figure 10: Reynolds stress (v'v')

With regard to second order statistics, the preliminary results show significant differences (e.g. see Figure 10), which could be due to the used mesh level and time-integration period. As the solutions of the pending cases become available with sufficient time-integration period, more light could be shed on the remaining topics of interest, like stratification, detailed turbulent statistics, heat transfer and fluid dynamics.

ACKNOWLEDGEMENTS

This work has been by financially supported by the Ministerio de Educación y Ciencia, Secretaría de Estado de Universidades e Investigación, Spain (ref. ENE2009-07689 and ENE2009-09496).

REFERENCES

[1] D. D. Gray and A. Giorgini. The validity of the boussinesq approximation for liquids and gases. *International Journal of Heat and Mass Transfer*, 19(5):545–551, 1976.

[2] D.G. Barhaghi and L. Davidson. Natural convection boundary layer in a 5:1 cavity. *Physics of Fluids*, 19:125106, 2007.

[3] X. Trias, M. Soria, A. Oliva, and C. D. Pérez-Segarra. Direct Numerical simulations of two and three dimensional turbulent natural convection flows in a differentialy heated cavity of aspect ratio 4. *Journal of Fluid Mechanics*, 586:259–293, 2007.

[4] S. Xin, J. Salat, P. Joubert, A. Sergent, and P. Le Quere. Three dimensional numerical simulations of turbulent natural convection in an air-filled differentially heated cavity. In *Proceedings of the 13th International Heat Transfer Conference*, 2006.

[5] D. Kizildag, J. Ventosa, I. Rodriguez, and A. Oliva. Non-Oberbeck-Boussinesq Natural Convection in a Tall Differentially Heated Cavity. In *Proceedings of the Fifth European Conference on Computational Fluid Dynamics ECCOMAS CFD 2010*, pages 1–13, 2010.

[6] M. Furukawa. Practical Expressions for Thermodynamic and Transport Properties of Commonly Used Fluids. *Journal of Thermophysics and Heat Transfer*, 5(4):524–531, 1991.

[7] R. W. C. P. Verstappen and A. E. P. Veldman. Symmetry-preserving discretization of turbulent flow. *Journal of Engineering Mathematics*, 187(1):343–368, 2003.

[8] G. M. Fishpool and M. A. Leschziner. Stability bounds for fractional-step schemes for the Navier-Stokes equations at high Reynolds number. *Computers and Fluids*, 38(6):1289–1298, 2009.

[9] Y. Morinishi, T.S. Lund, O.V. Vasilyev, and P. Moin. Fully conservative higher order finite difference schemes for incompressible flow. *Journal of Computational Physics*, 143(1):90–124, 1998.

[10] F. N. Felten and T. S. Lund. Kinetic Energy Conservation Issues Associated with the Collocated Mesh Scheme for Incompressible Flow. *Journal of Computational Physics*, 215(2):465–484, 2006.

[11] J. Patterson and J. Imberger. Unsteady natural convection in a rectangular cavity. *J. Fluids Mech.*, 100:65–86, 1980.

[12] J. Schmalzl, M. Breuer, and U. Hansen. On the validity of two-dimensional numerical approaches to time-dependent thermal convection. *Europhys. Lett.*, 67(3):390–396, 2004.